TOTAL SOLAR IRRADIANCE VARIATION DURING RAPID SUNSPOT GROWTH

H. JABRAN ZAHID[1], HUGH S. HUDSON[1] and CLAUS FRÖHLICH[2]
[1]*Space Sciences Laboratory, University of California, Berkeley, CA 94720, U.S.A.*
[2]*Physikalisch-Meteorologisches Observatorium Davos, World Radiation Center, Davos Dorf, Switzerland*

(Received 18 December 2003; accepted 23 March 2004)

Abstract. Large sunspot areas correspond to dips in the total solar irradiance (TSI), a phenomenon associated with the local suppression of convective energy transport in the spot region. This results in a strong correlation between sunspot area and TSI. During the growth phase of a sunspot other physics may affect this correlation; if the physical growth of the sunspot resulted in surface flows affecting the temperature, for example, we might expect to see an anomalous variation in TSI. In this paper we study NOAA active region 8179, in which large sunspots suddenly appeared near disk center, at a time (March 1998) when few competing sunspots or plage regions were present on the visible hemisphere. We find that the area/TSI correlation does not significantly differ from the expected pattern of correlation, a result consistent with a large thermal conductivity in solar convection zone. In addition we have searched for a smaller-scale effect by analyzing white-light images from MDI (the Michelson Doppler Imager) on SOHO. A representative upper-limit energy consistent with the images is on the order of 3×10^{31} ergs, assuming the time scale of the actual spot area growth. This is of the same order of magnitude as the buoyant energy of the spot emergence even if it is shallow. We suggest that detailed image analyses of sunspot growth may therefore show 'transient bright rings' at a detectable level.

1. Introduction

The pioneering high-precision observations of the total solar irradiance (TSI) showed that sunspots reduced the TSI approximately in proportion to their area (Willson *et al.*, 1981). The observations also showed that active regions can contribute positively to the TSI via facular excess emission (e.g., Hudson, 1988; Fröhlich, 2000). In fact, the facular excess contributions roughly balance the sunspot deficits over the lifetime of a large active region (Chapman, 1980), suggesting a physical link – is the facular emission simply the luminosity missing from the sunspots themselves? This possibility had encouraged searches for bright emission rings surrounding sunspots (Fowler, Foukal, and Duvall, 1983; Rast *et al.*, 2001; see also de Jager, 1959).

The basic theory of convective energy transport near the solar surface involves such efficient transport of energy that the sunspot deficit will simply diffuse throughout the convection zone and subsequently re-appear only on a time scale much longer than the lifetime of an active region (Spruit, 1977; Foukal, Fowler, and

Solar Physics **222:** 1–15, 2004.

Livshits 1983; Fox, Sofia, and Chan, 1991). The approximate equality of sunspot deficit and facular excess energies must be regarded as a coincidence in this theoretical framework. The theory also implies that steady-state bright rings resulting from diverted convective energy flow would not be very bright, which is consistent with the observations.

Another way to test this theory takes advantage of the fact that active-region time scales are comparable to the rotation period of the Sun. As a result the purely geometrical foreshortening of sunspot area and the actual physical growth of sunspot area must compete in defining the observed correlation between area and TSI. The physical growth would involve a thermal effect that one might detect in the correlation between area and TSI. For example the buoyant motion of a macroscopic flux tube corresponds to gravitational potential energy, and the conversion of some of this energy to heat via flows would cause local temperature anomalies and thus irradiance variations.

This paper reports a study of a rapidly-growing active region, NOAA 8179, which provides a first observational study regarding this idea (see also Hudson, Jones, and McIntosh, 1983). The sunspots grew just during central meridian passage (15 March 1998), at a time in which there were no other large sunspot groups on the disk. We have searched for an effect of the rapid growth on TSI directly (Section 3), and have also looked for a 'transient bright ring' that might have appeared near the spots during their growth (Section 4). We find no evidence for any irradiance effects of sunspot growth and discuss the upper limits resulting from this study.

2. Data

This study makes use of data from the Solar and Heliospheric Observatory (SOHO; see *http://sohowww.nascom.nasa.gov* for fuller details of the spacecraft and the instruments used). Specifically we use the white-light and magnetogram images from the Michelson Doppler Imager (MDI) to define sunspot areas as a function of time. The MDI provides images at 96-min intervals with $2''$ pixels. For TSI we use the data from the VIRGO instrument also on SOHO.

The MDI images have sufficient resolution to define sunspot umbra and penumbra regions, as shown in Figure 1. Note that the spot group grew rapidly just at the time of central meridian passage, with most of the area growth taking place on March 14. This gives us an optimum comparison between physical growth and area change via geometrical effects (foreshortening). The morphology of sunspot appearance followed a typical pattern: areas of each polarity appear independently and drift gradually apart with time after their first appearance. Figure 2 shows portions of the magnetograms to illustrate the morphology of magnetic flux growth.

We quantify the magnetic flux shown by the MDI images by integrating the positive and negative values over a region of interest of area $286'' \times 162''$. We

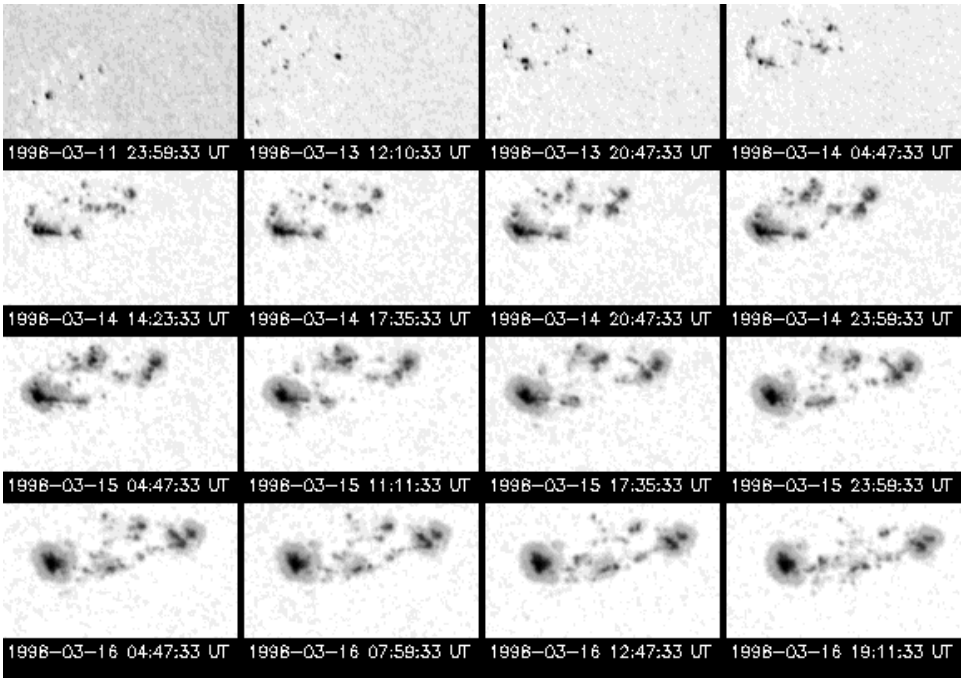

Figure 1. Time series of images showing the sudden growth of sunspots in NOAA active region 8179. These MDI sub-images are each $286'' \times 162''$ in area. In this figure and the next, N is up and W to the right.

show this in Figure 3 in comparison with the area of the sunspots in AR 8179 (see Section 3). The integrations begin at one gauss, following the calibration provided by the MDI team. We have not considered calibration uncertainties (see Berger and Lites, 2003) that might affect the greater concentration of field into the sunspots. Nevertheless, Figure 3 shows that the time evolution of the magnetic field differs considerably from that of the spot area; the growth of the magnetic flux precedes the spot growth. This can also be seen in the comparison of Figures 1 and 2. The magnetism appears to be less sharply defined than the spots.

3. Sunspots and Faculae

3.1. Sunspot areas and PSI

The effects of sunspots and faculae on the TSI are often modeled via the use of a PSI (Photometric Sunspot Index; see Hudson *et al.*, 1982) and PFI (Photometric Facular Index; see Chapman and Meyer, 1986; Chapman, 1987). The essential idea of these indices is to make use of image data to characterize the active-region effects. If only these perturbations of the TSI were present, the residuals between

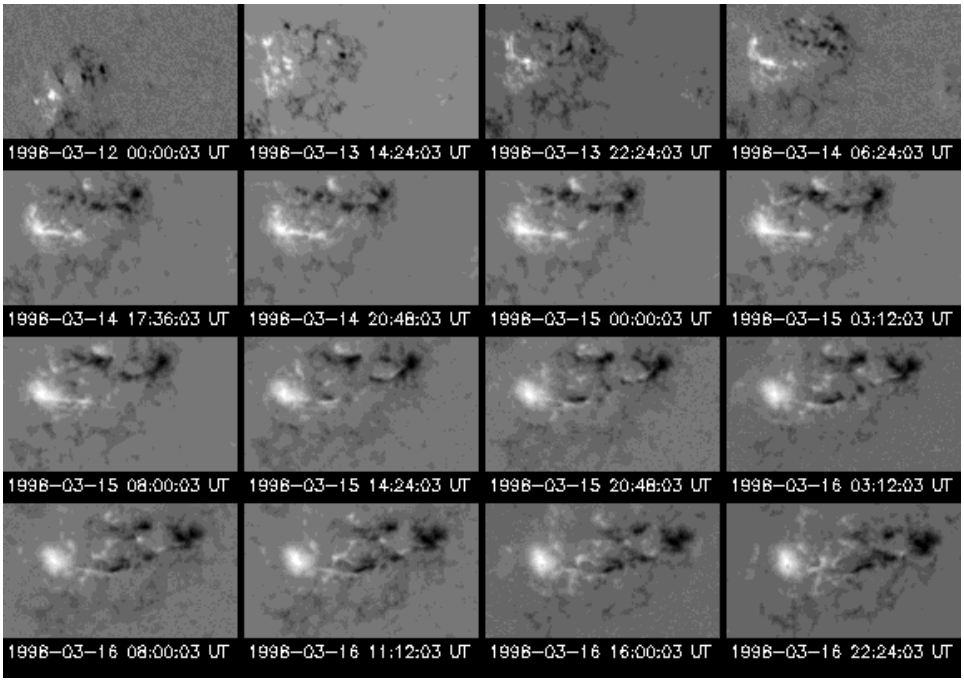

Figure 2. Time series of images showing the MDI magnetic fluxes for the same regions, at 30 sec displacements from the white-light images except for the second item. The lighter regions represent positively polarized magnetic field, and the darker spots represent the negatively polarized magnetic field.

the TSI and these corrections should result in an unvarying residual time series. In studying the asymmetry of the area/TSI correlation, the observational goal of this study, we use PSI and PFI estimates to reduce the uncertainties due to the presence of competing active regions.

As can be seen from Figure 4, region 8179 grew rapidly; the area grew within half a day on 14 March: $\tau = dt/d(\ln A) \sim 14$ h. Prior to this eruption other smaller regions dominated the total sunspot area. Their areas remained small and changed only slowly, however, during the remainder of 8179's lifetime on the visible hemisphere.

The first step in modeling the sunspot effects is to estimate the areas by use of the MDI images (see also Ortiz *et al.*, 2002, and Turmon, Pap, and Mukhtar, 2002, who have in addition made use of the MDI magnetograms to estimate facular effects). We have done this by correcting for limb darkening in the images and then by imposing a fixed fractional intensity threshold. Establishing a threshold for this kind of measurement is not straightforward. Our choice here, 87% of the local quiet photospheric intensity, resulted in areas close to those tabulated by NOAA. Figure 4 shows the results of this procedure, in comparison with the areas for the other four sunspot groups present during this time. This figure clearly shows the

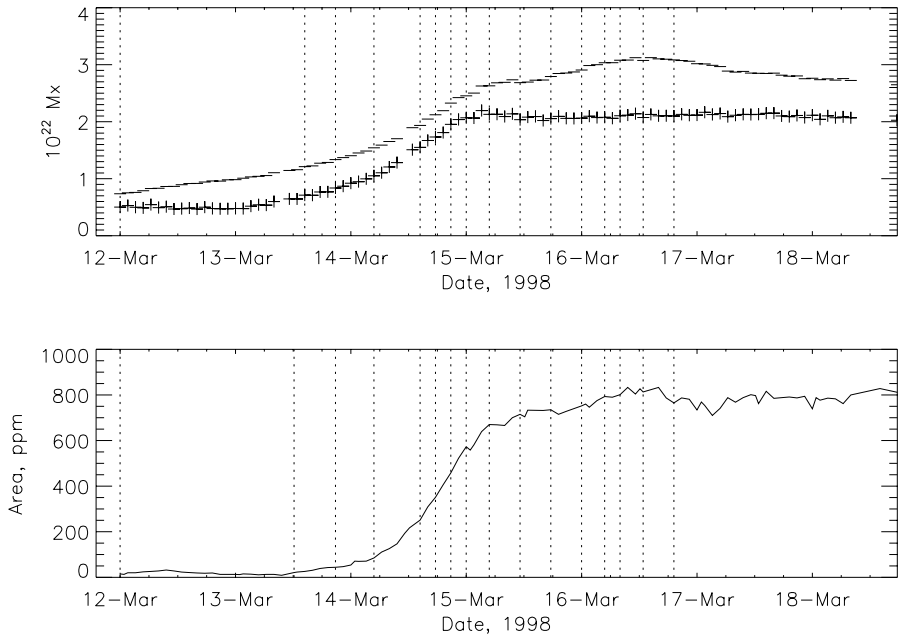

Figure 3. Top panel: the positive and negative magnetic fluxes as a function of time. The *plus signs* show the positively polarized field, and the *minus signs* show the absolute value of the negatively polarized field. *Bottom panel*: time series of sunspot area. The *vertical dotted lines* show the image times for Figures 1 and 2.

merits of the MDI observations (regular and frequent sampling; good precision) for this kind of application.

Figure 4 compares the sunspot group areas we have derived from the MDI observations with those of Ramey, one of the NOAA source observatories. The areas that we calculate for the larger sunspots match well with the Ramey data. For the smaller areas we see fluctuating and systematic differences between the Ramey measurements and ours, as illustrated in Table I. The random fluctuations – relatively greater for the smaller spots – presumably result from the relative importance of pixelization errors, as well as from photometric errors due to p-mode oscillations and other sources of small-scale intensity variation. The NOAA data sources, such as Ramey, report only one measurement per day, so we cannot readily compare RMS uncertainties.

The simplest definition of PSI (Hudson *et al.*, 1982) is given by

$$\Psi = \frac{\Delta S_s}{S_\odot} = \alpha \sum \mu A_s \frac{3\mu + 2}{2}; \tag{1}$$

here the summation is over all the sunspot regions present on the disk. This gives PSI in parts per million of the solar constant $S_\odot$ (TSI). As usual $\mu = \cos(\theta)$ where

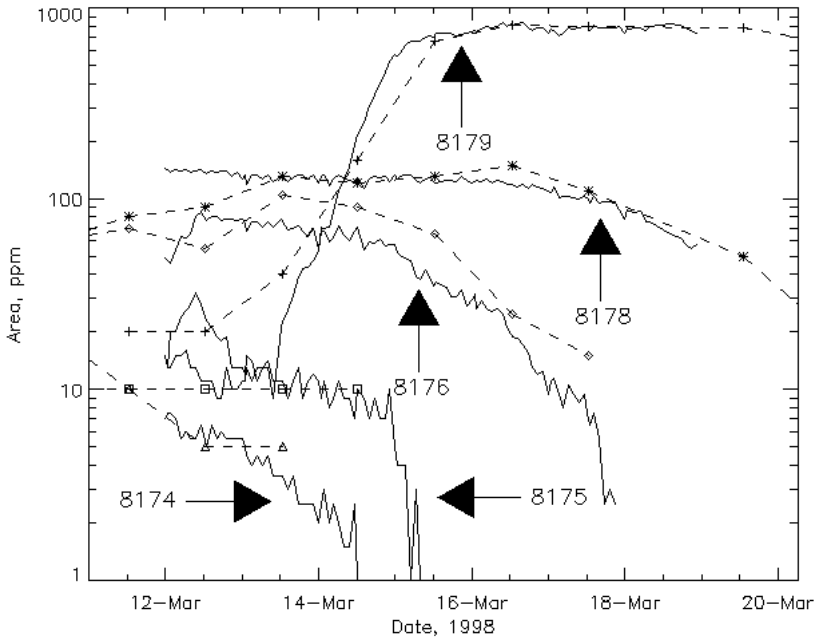

Figure 4. Sunspot areas on a semi-log representation, with the *solid lines* showing our estimates from MDI data. Routine NOAA daily estimates of region areas (from Ramey observations) are given by different symbols: plus, 8179; asterisk, 8178; diamond, 8176; square, 8175; triangle, 8174. To avoid confusion we have reduced the areas of 8174 and 8176 by a factor of two. Areas are given in parts per million (ppm) of a solar hemisphere and are corrected for foreshortening.

TABLE I

RMS noise levels for representative MDI spot areas.

NOAA region	Date 1998	NOAA area	MDI area	MDI RMS
8179	16 March	900	900	10
8175	13 March	10	21.1	4

θ is the angle between the center of the sunspot and the solar normal; A_s is the area of the spot corrected for foreshortening, as we calculated earlier. The 'bolometric constant' α (Chapman, Cookson, and Dobias, 1994) is given by

$$\alpha = \frac{A_u}{A_s}\left[1 - (\frac{T_u}{T_0})^4\right] + \frac{A_{pu}}{A_s}\left[1 - \left(\frac{T_{pu}}{T_0}\right)^4\right]. \quad (2)$$

Here A_u, A_{pu}, T_u, and T_{pu} are the umbral and penumbral areas and temperatures respectively and T_0 is the effective temperature of the photosphere.

A physically more realistic model for PSI is one described by Steinegger *et al.* (1996), as proposed by Steinegger *et al.* (1990). In this model α is no longer a constant but instead is derived from the spatial distribution of intensities within a region:

$$\Psi = \frac{\Delta S_s}{S_\odot} = \sum \alpha \mu A_s \frac{3\mu + 2}{2}. \tag{3}$$

Here the summation is over all sunspot groups. The value of α for a given pixel is given by

$$\alpha = \sum_i \frac{A_i}{A_s} \left[1 - \left(\frac{T_i}{T_0} \right)^4 \right], \tag{4}$$

where the summation is over single pixels. The temperature T_i can be found from the monochromatic intensity contrast $I_i(\lambda)/I_0(\lambda)$ and Planck's Law, giving (Bray, 1981)

$$T_i = \frac{c_2}{\lambda} \left(\ln \left[\left(e^{\frac{c_2}{\lambda T_0}} - 1 \right) \frac{I_i(\lambda)}{I_0(\lambda)} + 1 \right]^{-1} \right); \tag{5}$$

here T_0 is 6097 K as given by Steinegger *et al.* (1990).

We use a small refinement of this method. In the Steinegger version a constant μ is adopted for each sunspot, although a given group may cover a range of values of μ. By combining Equations (3) and (4) we get

$$\Psi_s = \sum_i A_i \left[1 - \left(\frac{T_i}{T_0} \right)^4 \right] \frac{3\mu_i + 2}{2}, \tag{6}$$

where Ψ_s is the PSI for an individual sunspot and the index i extends over all pixels in the sunspot. Here, neither α (which depends upon the T_i) nor μ_i are constant. To get the total PSI we then take

$$\Psi = \sum_s \Psi_s, \tag{7}$$

where now the summation is over the sunspot groups. The resulting PSI is shown in the upper panel of Figure 5.

3.2. FACULAE AND PFI

The other known major contribution to TSI variation comes from the faculae, which we model using a Photometric Facular Index. Chapman and Meyer (1986) and Chapman (1987) define PFI as

$$\Phi = \frac{\Delta S_f}{S_\odot} = C'_p \sum A_p \mu f(\mu) \xi(\mu), \tag{8}$$

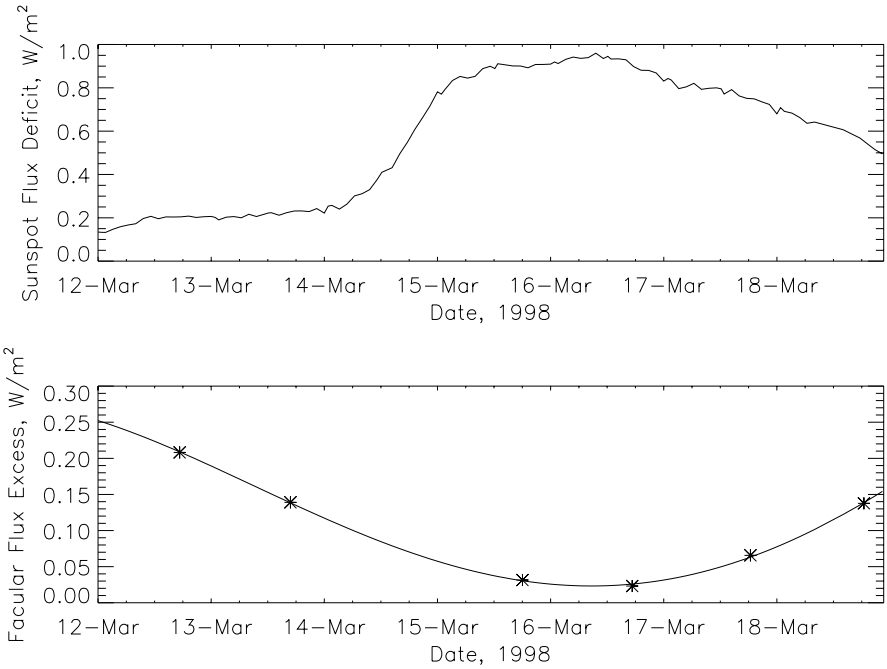

Figure 5. Top panel: PSI calculated from the MDI white-light images (110 over this time span). *Bottom panel*: PFI calculated from 8 Ca II images obtained from Big Bear Solar Observatory. The *solid line* shows a fourth-degree polynomial fit.

where the summation extends over all plage regions. $f(\mu)$ is the limb-darkening law and $\xi(\mu)$ is the facular contrast function. The constant C'_P is an empirically determined constant. Chapman (1980) gives $\xi(\mu) = b(\mu^{-1} - a)$ and the limb-darkening law is given by $f(\mu) = (3\mu + 2)/5$.

Following Chapman (1987) we obtain

$$\Phi = C_p \sum A_p(3\mu - 3a\mu^2 + 2 - 2a\mu), \tag{9}$$

where $C_p = 0.0185$ (Chapman and Meyer, 1986) and $a = 1$ for zero contrast at disk center. Figure 5 shows the results of this calculation. If we add the PSI to the TSI and subtract the PFI from the TSI, then we should recover the quiet-Sun irradiance.

An estimate of PFI requires plage areas, and we found only three entries in the *Solar–Geophysical Data* (*SGD*). Accordingly we also estimated plage areas by direct area estimates based upon Ca II images from Big Bear Solar Observatory. The images obtained from BBSO were already dark-corrected and flat-fielded. The areas were calculated by setting an lower limit threshold for plage. These BBSO areas were then calibrated by comparing results with the areas given in the SGD.

We now apply both corrections to the TSI time series, as shown in Figure 6. The residuals should in principle be flat and unvarying. Instead we see a slight upward

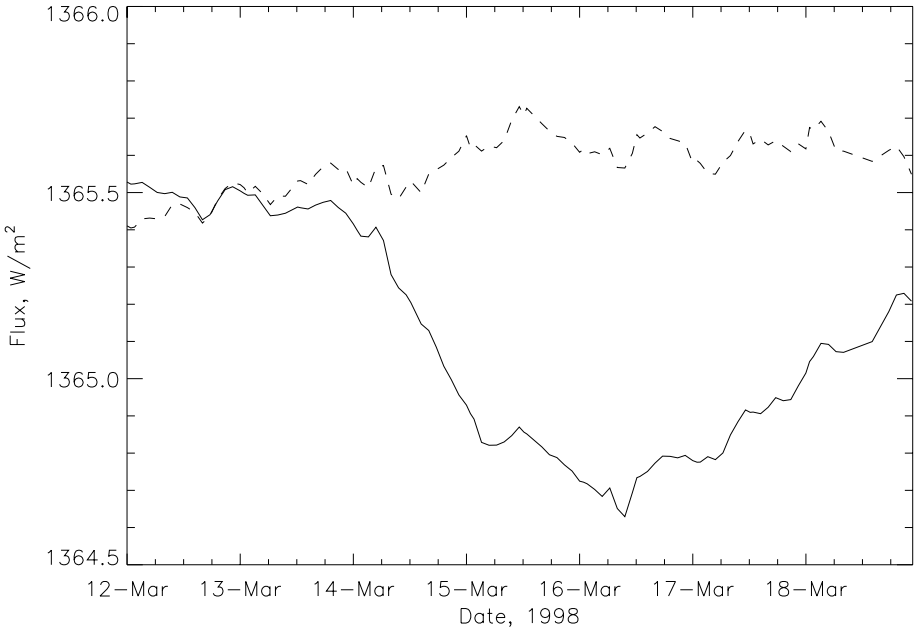

Figure 6. TSI variation with and without the corrections (PSI and PFI) for sunspots and faculae, as described in the text.

trend of roughly 0.2 W m^{-2} (150 ppm) plus broad-band low-frequency noise of some tens of ppm. This trend probably reflects incomplete corrections for spots and faculae, plus the contribution of the 'active network' (e.g., Foukal and Lean, 1988) which we have not included in our corrections. The residuals show no clear correlation with the PSI (sunspot area variation), but do exhibit small fluctuations (of order 0.1 W m^{-2}) of unknown origin.

The time series of PSI and TSI, the data necessary for the correlation studied below, appears in Figure 7. Note the additional variability in the TSI, on short timescales, above that seen in the PSI correction. This component is not seen in the sunspot areas derived from the white-light images and therefore reflects a variation term in the TSI itself.

3.3. THE AREA/TSI CORRELATION

We are now prepared to characterize the correlation between area variation in AR 8179 and the TSI. We make the PSI corrections for the other regions, and the PFI corrections for all regions. The result is shown in Figure 8 which separates the two branches for clarity. The first branch is the growth phase of the sunspot, with a decreasing TSI; the second is the recovery, dominated by rotation and foreshorten-

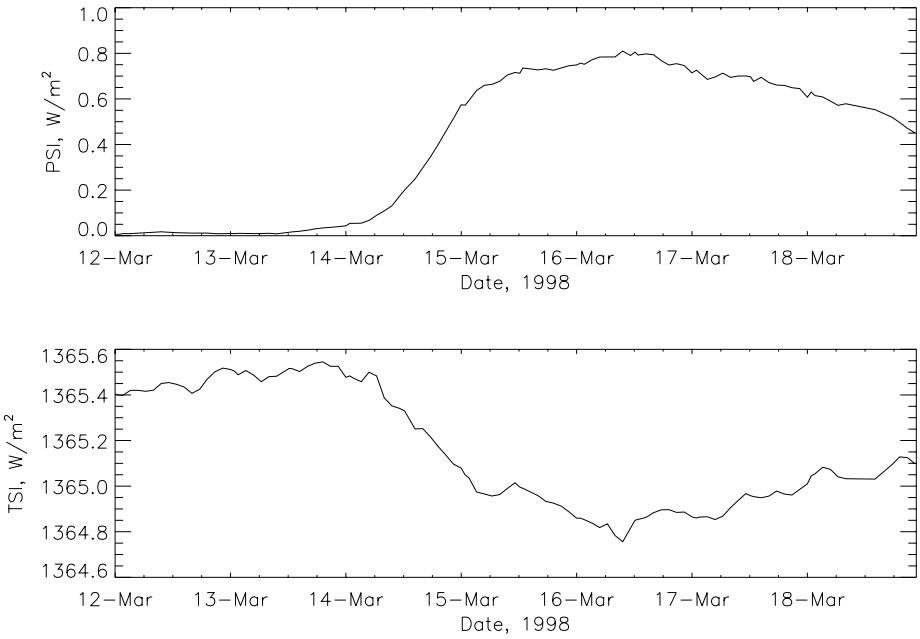

Figure 7. The data used for analysis of correlation between PSI (*upper*) and corrected TSI (*lower*) as time series. The TSI corrections consist of the deficits from the other regions and from PFI. Note the additional short-term variability in the TSI.

TABLE II
Fits to PSI/TSI variations.

Phase	PSI = 0.6 W m^{-2}	Slope
Increasing branch	1365.07	−0.79
Decreasing branch	1365.05	−0.89

ing of the sunspot group as it approaches the limb. Linear fits for the two branches of the correlation are shown in Figure 8, with parameters given in Table II.

3.4. Analysis of the upper limit

The basic result of our analysis, the correlation plot shown in Figure 8, shows that the rapid growth of a large sunspot group has no apparent thermal effects that we can detect via the TSI measurements.

We are unaware of any detailed theoretical or model predictions of a thermal effect to compare with this observation, and so we make a crude dimensional estimate here of the possible magnitude of a thermal effect. This assumes the form-

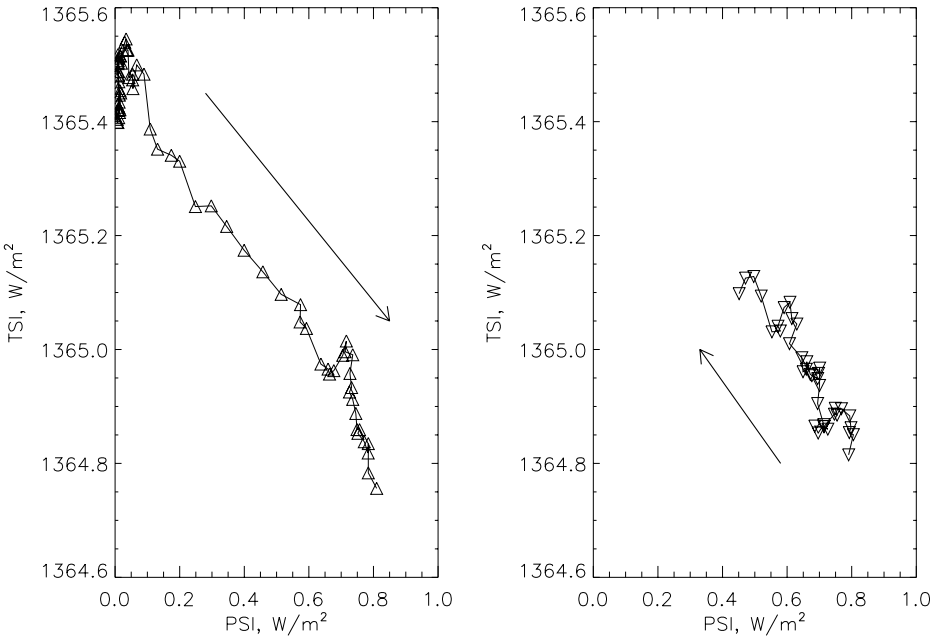

Figure 8. The correlation between the PSI and TSI in its two branches. The *arrows* show the growth phase (*left*) and the decay phase (*right*): the former due to physical growth and the latter to geometrical foreshortening. The striking feature near the end of the growth phase, at a TSI value near 1365 W m^{-2}, is due to the TSI itself and not to the PSI correction, and can also be seen as part of the time-series variability in Figure 7.

ation of the sunspot group by the buoyant motion of a large-scale flux tube through the photosphere, with the amount of gravitational energy implied by this buoyant motion. The image sequences shown in Figures 1 and 2 are roughly consistent with this scenario. Taking a characteristic length scale $L = \sqrt{A_{\text{group}}}$ for the vertical motion, where A_{group} represents the area of the sunspot group, the buoyant energy is of order $L^3 \times \rho g_\odot D$, with ρ the density and $g_\odot = 2.7 \times 10^4$ cm s^{-2}. Thus the gravitational potential energy W_{buoy} involved in the eruption can be estimated as

$$W_{buoy} = L^4 \rho g_\odot / \tau, \tag{10}$$

where $\tau = dt/d\ln(A)$ is the growth time of the spot group, approximately 5×10^4 s for NOAA 8179. We have simply set $D = L$ for this estimate. From Allen (1973) we take $\rho = 10^{-4} D_9$, where D_9 is the depth in units of 10^9 cm. The dimension L of the spot group is about 5×10^9 cm, so taken at face value one finds a total energy $W_{buoy} \sim 10^{39}$ ergs (Table III). Another assumption might be that the vertical buoyant motion would only correspond to the scale of the Wilson depression (Wilson and Maskelyne, 1774; see Wilson and Cannon, 1968). In this case the available energy would drop to about $W_{buoy} \sim 10^{33}$ ergs, assuming a sunspot depth

of only 10^8 cm and a correspondingly low density. We conclude from this that the buoyant motion in principle involves a large amount of energy, but that it depends in detail upon the structure of the magnetic field prior to its eruption. Another major uncertainty in these estimates is the efficiency of conversion to luminosity, which depends upon the details of the flow field that results from the eruption and upon ill-understood physical parameters such as the thermal conductivity near the solar surface.

4. Transient Bright Ring

In this section we describe a rudimentary direct search in the white-light images for a thermal effect. This approach would be more sensitive if the energy conversion occurs locally. The idea here is that a luminous 'transient bright ring' (TBR) would appear on small spatial scales at the time of sunspot eruption, as a direct result of flows associated with the eruption. Here we estimate a lower limit on how luminous such a transient bright ring would have to be in order to be detectable. We investigate the local region around AR 8179 by considering the image histogram in the MDI image sub-regions as shown in Figure 1.

A transient bright ring would result from the sunspot growth, so we model its time history by differentiating the area increase and then doing a standard Gaussian fit. This is illustrated in Figure 9; the Gaussian peak gives a reasonable fit to the area growth even though it is just a mathematical convenience.

If we suppose that our model crudely describes the behavior of the transient bright ring then we must find an amplitude for our Gaussian fit that would allow us to see such an effect. The bright ring effect appears as a brightening in some pixels and produces a time-series effect in the positive branch of the image histogram, i.e. those pixels brighter than the quiet photosphere. A model[1] amplitude that allows us to witness this effect against the observed irradiance variability then gives an estimated limit.

In order to estimate the limit we must convert the amplitude of the Gaussian into absolute intensity units used in our MDI images and from this we can convert into luminosities. We start with intensities in our local region that were above quiet-sun levels and then normalize them to the brightness of a mirror-image region N of the solar equator, thus making a differential measurement. Figure 10 shows a range of Gaussian models for the time variation of the bright-ring flux overlaid on the observed variation of the total flux above quiet-Sun level (positive pixel brightnesses). The individual curves correspond to 1.5, 3, and 6×10^{31} ergs when integrated over the Gaussian time profile. A model incorporating energy storage would result in a time lag and a smaller amplitude; the upper limit would be larger for such a model, which we do not consider here.

[1] In the model, we have set all the negative values of the time derivative to zero.

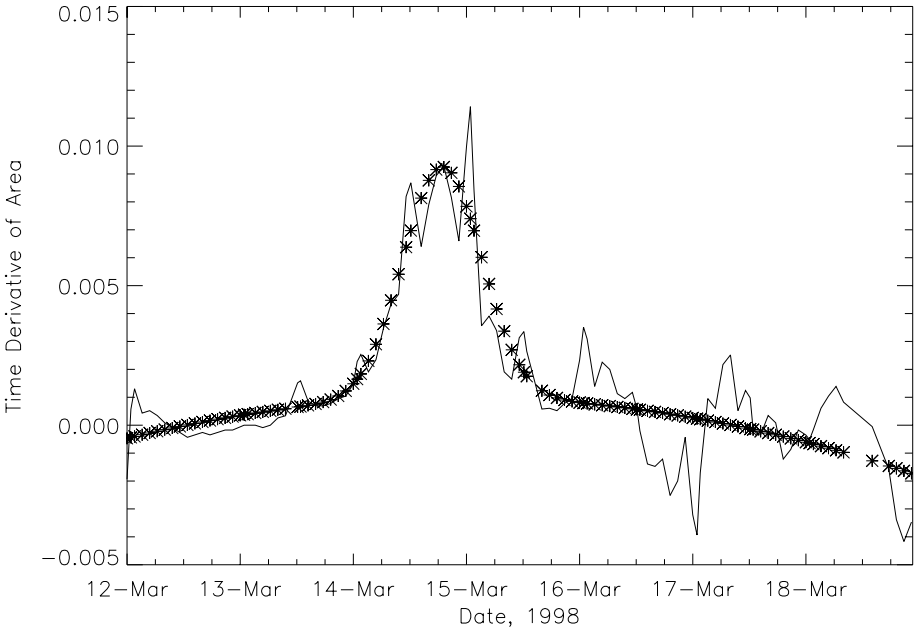

Figure 9. Time derivative of area growth (*solid line*), with an overlaid Gaussian fit (*asterisks*) to represents our simplified model for the time variation of intensity for a transient bright ring.

5. Conclusions

We have studied an isolated large sunspot group that grew rapidly at disk center, searching in two ways for irradiance (luminosity) changes that might be associated with the physical process of sunspot formation. Such an effect is hypothetical and should be distinguished from the 'sunspot blocking' effects clearly seen in TSI observations, which relate to the steady state. It does not seem implausible that transient luminosity effects should exist, since it is generally accepted that sunspot fields result from the emergence through the photosphere of buoyant flux tubes, which involves flows and gravitational energy. We encourage the development of a theory of solar magnetic flux eruption and sunspot formation that can describe the associated irradiance variations. These effects may depend upon the nature of the sunspot group; Lites *et al.* (1995) find that a delta configuration may erupt in a characteristic manner.

We find that the correlation between sunspot area (via PSI) and the total solar irradiance matches during the two distinct phases, which represent actual physical growth and purely geometrical foreshortening respectively. In principle a thermal effect should be expected to occur during the growth phase, because of the energy involved in buoyancy and in magnetic effects. This therefore represents an independent test of theories of thermal energy redistribution in the upper convection

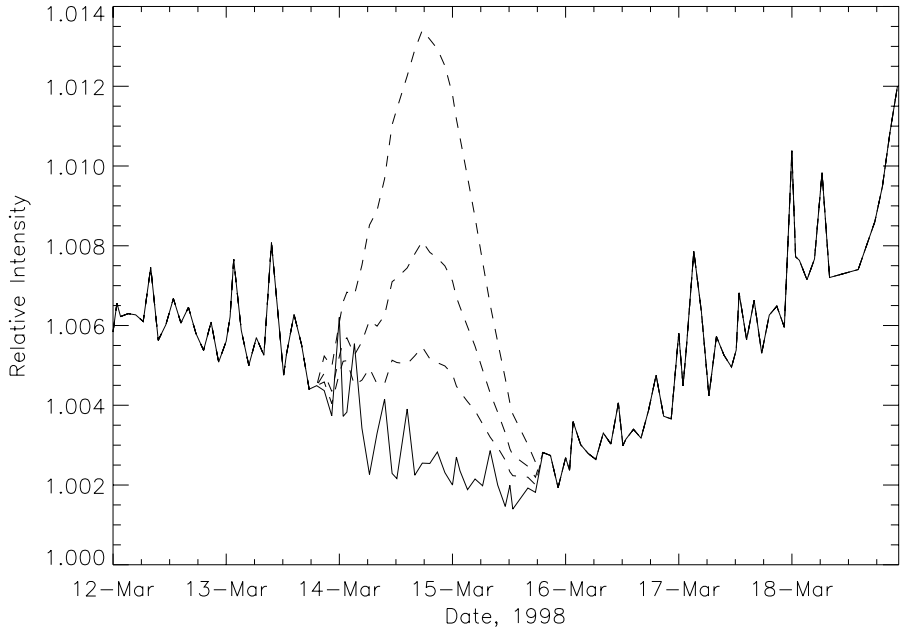

Figure 10. Sum of positive pixel brightnesses for the image sub-region; the *dashed lines* show hypothetical signals proportional to the time profile shown in Figure 9. We use these to estimate an upper limit on a signal from the hypothetical transient bright ring. The lines correspond to 1.5, 3, and 6×10^{31} ergs, respectively.

TABLE III

Limits on transient irradiance effects.

Limit from TSI analysis	10^{33} ergs
Limit from TBR analysis	3×10^{31} ergs
W_{buoy} estimate from full depth	10^{39} ergs
W_{buoy} estimate from Wilson depression	10^{33} ergs

zone. Our observational result is an upper limit on the magnitude of this effect, which for a sunspot of this size and rapidity of growth could be detectable in TSI in the absence of rapid convective dissipation of the excess energy. The lack of an observable effect is consistent with the expectations from the standard theory (Spruit, 1977) of thermal redistribution in the solar interior. This theory will break down eventually on small spatial scales and short time scales, so high-resolution observations should be a focus for future searches. The order of magnitude of the effect may increase rapidly with the spatial scale of the spot, $\Delta L \sim D^4$. A further

study of rapidly-growing large spots making use of detailed image analysis at the highest possible angular resolution therefore may be required to detect any thermal effects of the eruption process.

Acknowledgements

The work of HJZ and HSH was supported by the DoD MURI grant 'Understanding Magnetic Eruptions on the Sun and their Interplanetary Consequences.' We thank the Big Bear Solar Observatory and MDI groups for making their data available, and also thank Dave Bercik for reading and commenting.

References

Allen, C. W.: 1973, *Astrophysical quantities*. London: University of London, Athlone Press, 3rd ed.
Berger, T. E. and Lites, B. W.: 2003, *Solar Phys.* **213**, 213.
Bray, R. J.: 1981, *Solar Phys.* **69**, 3.
Chapman, G. A.: 1980, *Astrophys. J. Lett.* **242**, L45.
Chapman, G. A.: 1987, *J. Geophys. Res.* **92**, 809.
Chapman, G. A. and Meyer, A. D.: 1986, *Solar Phys.* **103**, 21.
Chapman, G. A., Cookson, A. M., and Dobias, J.J.: 1994, *Astrophys. J.* **432**, 403.
de Jager, C.: 1959, *Handbuch der Physik* **52**, 80.
Foukal, P. and Lean, J.: 1988, *Astrophys. J.* **328**, 347.
Foukal, P., Fowler, L. A., and Livshits, M.: 1983, *Astrophys. J.* **267**, 863.
Fowler, L. A., Foukal, P., and Duvall, T.: 1983, *Solar Phys.* **84**, 33.
Fox, P. A., Sofia, S., and Chan, K. L.: 1991, *Solar Phys.* **135**, 15.
Fröhlich, C.: 2000, *Space Sci. Rev.* **94**, 15.
Hudson, H. S.: 1988, *Ann. Revs. Astron. Astrophys.* **26**, 473.
Hudson, H. S., Jones, H., and McIntosh, P.: 1983, *Bull. Am. Astron. Soc.* **15**, 950.
Hudson, H. S., Silva, S., Woodard, M., and Willson, R.C.: 1982, *Solar Phys.* **76**, 211.
Lites, B. W., Low, B. C., Martinez Pillet, V., Seagraves, P., Skumanich, A., Frank, Z. A., Shine, R. A., and Tsuneta, S.: 1995, *Astrophys. J.* **446**, 877.
Ortiz, A., Solanki, S. K., Domingo, V., Fligge, M., and Sanahuja, B.: 2002, *Astron. Astrophys.* **388**, 1036.
Rast, M. P., Meisner, R. W., Lites, B. W., Fox, P. A., and White, O. R.: 2001, *Astrophys. J.* **557**, 864.
Spruit, H. C.: 1977, *Solar Phys.* **55**, 3.
Steinegger, M., Brandt, P. N., Schmidt, W., and Pap, J.: 1990, *Astrophys. Space Sci.* **170**, 127.
Steinegger, M., Vazquez, M., Bonet, J. A., and Brandt, P. N.: 1996, *Astrophys. J.* **461**, 478.
Turmon, M., Pap, J. M., and Mukhtar, S.: 2002, *Astrophys. J.* **568**, 396.
Willson, R. C., Gulkis, S., Janssen, M., Hudson, H. S., and Chapman, G. A.: 1981, *Science* **211**, 700.
Wilson, A. and Maskelyne, N.: 1774, *Phil. Transactions Series I* **64**, 1.
Wilson, P. R. and Cannon, C. J.: 1968, *Solar Phys.* **4**, 3.